Modelling of a Hybrid Energy System for Autonomous Application

Regular Paper

Yang He[1], Zheng You[1] and Xiaofeng Wang[1,*]

1 State Key Laboratory of Precision Measurement Technology and Instruments, Tsinghua University, China
* Corresponding author E-mail: xfw@mail.tsinghua.edu.cn

Abstract A hybrid energy system (HES) is a trending power supply solution for autonomous devices. With the help of an accurate system model, the HES development will be efficient and oriented. In spite of various precise unit models, a HES system is hardly developed. This paper proposes a system modelling approach, which applies the power flux conservation as the governing equation and adapts and modifies unit models of solar cells, piezoelectric generators, a Li-ion battery and a super-capacitor. A generalized power harvest, storage and management strategy is also suggested to adapt to various application scenarios.

Keywords Hybrid Energy, Autonomous System, Solar Cell, Piezoelectric, Li-ion Battery, Super-Capacitor

1. Introduction

Stand-alone or autonomous systems, such as wireless sensor networks [1] and flapping wing robotic insects [2], require an off-grid power supply with a high sustainability, stability and reliability. Current practice usually applies a harvester to transform a single source of environmental energy to electrical power, such as solar or vibration [3], whose supply is highly restricted by the environmental

conditions and results in an abrupt failure due to a sudden inconvenience of climate. Hybrid energy systems (HES) are one of the most promising solutions and combine different environmental energies and enhance power reliability. An HES consists of a combination of energy harvesters and also storage units such as a rechargeable battery and a super-capacitor to reduce power loss.

Current HES research usually focuses on the direct development of the hardware equipment or prototype and then a forwarding test to verify the feasibility [4], which is of very low efficiency and reproducibility to other kinds of HES. HES modelling can eventually reduce the time and cost, and more importantly guide all kinds of hardware development through advice on choosing device parameters.

Many unit models are thoroughly developed, such as the one/two diodes model of a solar cell [5-7], the spring-mass-damp model of mechanical vibration generators [8-10], the PNGV model of a Li-ion battery [13-15] and the RC-network model of a super-capacitor [17-19]. Although these models provide high accuracy of simulation, it is barely reported of system models of HES adapting them, mainly because they aim to simulate each unit device performance from different aspects. In the

following article, a HES model is suggested by adapting these unit models into a power flux system.

2. General Model of Hybrid Energy System

The proposed HES model consists of four modules: an energy harvester, energy storage, management and energy output. In this paper, the harvesters are a combination of a solar cell and a piezoelectric generator, and a Li-ion battery and a super-capacitor serve as the storage units, as shown in Figure 1.
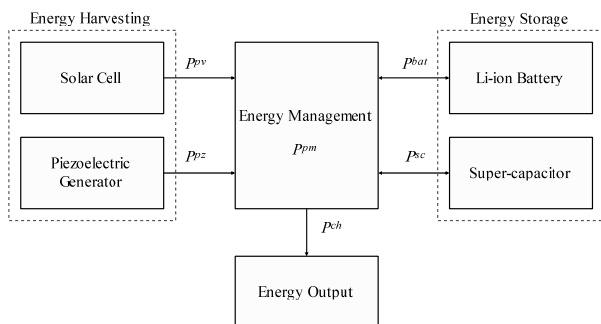

Figure 1. Hybrid energy system model

The governing equation of the general system model (Equation 1) is based on the principle of energy conservation.

$$P^{pv}+P^{pz}+P^{bat}+P^{sc}=P^{pm}+P^{ch} \tag{1}$$

P^* is the power flux of each module in Figure 1. $P^{bat}, P^{sc} > 0$ indicates the discharge of the battery and capacitor. Other harvesters and storages can eventually be added to the model to form a more hybrid energy supply system, once the unit models of the relative device are developed with an output of power flux.

3. Energy Harvesting Module

3.1 Photovoltaic (Solar Cell) Model

The single diode equivalent circuit [7], as shown in the dotted box in Figure 2, is applied to develop the current-voltage characteristic equation of a solar cell (Equation 2).

$$I_c = I_L - I_{sat} \left[\exp\left(\frac{V_c + I_c R_s}{\alpha}\right) - 1 \right] - \frac{V_c + I_c R_s}{R_p} \tag{2}$$
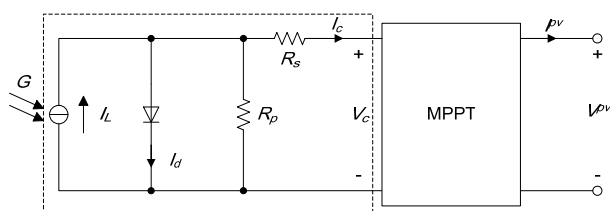

Figure 2. Solar cell model – single diode circuit

Five parameters are included in the model: I_L - the light current, I_L - the diode reverse saturation current, α - the ideality factor and R_p and R_s - shunt and series resistance. They are a function of the environmental conditions, involving irradiance G, junction temperature T_j and air mass AM (in form of correction factor M/M^*). Considering R_p and R_s as constant, the other three parameters can be interpreted by Equation 3-5, where * indicates the value under SRC (Standard Rating Conditions, with G^*=1000W/m2, T_j^*=25⊚ and AM^*=1.5), n_s is the series cell numbers in one module, E_g is the gap energy of cell material and K_I is the temperature coefficient of the short circuit current. [6]

$$\alpha = \frac{T_j}{T_j^*}\alpha^* \tag{3}$$

$$I_{sat} = I_{sat}^* \left(\frac{T_j}{T_j^*}\right)^3 \exp\left(\frac{n_s E_g}{\alpha^*}\left(1 - \frac{T_j^*}{T_j}\right)\right) \tag{4}$$

$$I_L = I_L^* \left(\frac{G}{G^*}\right)\left(\frac{M}{M^*}\right)\left(1 + K_{I_{sc}}\left(T_j - T_j^*\right)\right) \tag{5}$$

After the identification of the five model parameters, the module introduces a determination process for maximal power point aiming to simulate the MPPT (Maximal Power Point Tracker) and to provide the output power of solar cell module P^{pv}. At the MPP, an additional equation is available:

$$\frac{I}{V} = \left(1 - \frac{IR_s}{V}\right)\left(\frac{I_{sat}}{\alpha}\exp\left(\frac{V + IR_s}{\alpha}\right) + \frac{1}{R_p}\right) \tag{6}$$

From Equation 2 and 6, the maximal power point (I_{mp}, V_{mp}) can be calculated and eventually the output power:

$$P^{pv}=I_{mp}V_{mp} \tag{7}$$

3.2 Piezoelectric Generator Model

The piezo-generator is commonly in the form of a bimorph cantilever and is based on the 31-mode (or transverse) piezoelectric effect [3]. The equivalent circuit can be illustrated as shown in Figure 3 and the piezoelectric effect is simulated with a transformer [9].
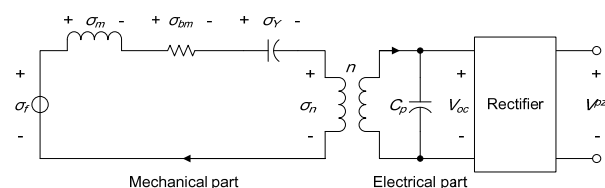

Figure 3. Piezoelectric generator model – transformer circuit

The governing equations of the vibration and piezoelectric effect are then deducted from the equivalent circuit as in Equation 8 and 9 [9, 10].

$$\ddot{\delta}_c + \frac{b_m b^{**}}{m}\dot{\delta}_c + \frac{Y_c b^* b^{**}}{m}\left(1 + \frac{d_{31}^2 Y_c}{\varepsilon_c}\right)\delta_c = \mu_1 b^* \ddot{y} \qquad (8)$$

$$\dot{V}_{oc} = -\frac{d_{31} Y_c h_c}{\varepsilon_c}\dot{\delta}_c \qquad (9)$$

$\delta_c(t)$ - strain in piezo-ceramic layer, $\ddot{y}(t)$ - environment vibration acceleration (on the fixed end of the cantilever beam), d_{31} - strain constant of the ceramic, Y_c - Young's modulus of the ceramic, ε_c - dielectric constant of the ceramic, h_c - thickness of the ceramic layer, m - free end mass weight, b^* and b^{**} - geometrical factors of the beam, determined by Equation 10 and 11, where l_b, l_c and l_m stand respectively for the length of whole beam, free end mass block and the ceramic layer, d is the distance between the layers of ceramic and substrate in the beam, and I_b is the effective inertia moment of the beam [11].

$$b^* = \frac{6d(2l_b + l_m - l_c)}{l_b(4l_b^2 + 6l_m l_b + 3l_m^2)} \qquad (10)$$

$$b^{**} = \frac{2I_b}{d(2l_b + l_m - l_c)} \qquad (11)$$

Equation 8 involves μ_1, the mass correction coefficient, to compensate the beam weight effect on vibration. μ_1 can be calculated from Equation 12, where λ is the linear weight of the beam [10].

$$\mu_1 = \frac{(m/\lambda l_b)^2 + 0.603(m/\lambda l_b) + 0.08955}{(m/\lambda l_b)^2 + 0.4637(m/\lambda l_b) + 0.05718} \qquad (12)$$

On solving the differential equations of Equation 8 and 9, the open circuit voltage $V_{oc}(t)$ can be identified. In case of a continuous harmonic excitation, $V_{oc}(t)$ will also be in sinusoidal form, noting the amplitude as V_m.

A rectifier serves after the piezoelectric generator to properly supply the load. It's proven that in a scenario with both Full-Bridge (FB) and Voltage-Doubler (VD) rectifier, the maximal power of the final output is determined by Equation 13, where ω is the excitation frequency, C_p is the equivalent parallel capacitor and w_b is the width of the beam [12].

$$P^{pz} = P_{max}^{pz} = \frac{C_p \omega V_m^2}{2\pi} \qquad (13)$$

$$C_p = \frac{\varepsilon_c w_b l_c}{h_c} \qquad (14)$$

4. Energy Storage Module

4.1 Li-ion Battery Model

The PNGV model is widely used in rechargeable battery simulation, as shown in Figure 4 [13]. V_{oc} is the static open circuit voltage. Resistance R_o reflects the ohmic polarization effect, while resistance R_p and capacitor C_p express the combined effect of electrochemical and concentration polarization. Capacitor C_b interprets the gradual variation of battery voltage.
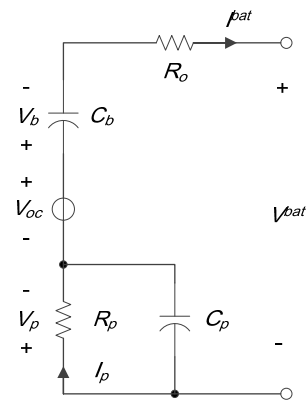

Figure 4. Li-ion battery model – PNGV circuit

The governing equations of the PNGV model are Equation 15-18 in a discrete form, where k is the order of sample data. The five parameters V_{oc}, R_o, R_p, C_p and C_b, included by the model, are a function of SoC, state of charge [15]. These relationships can be determined from the regular HPPC (Hybrid Pulse Power Characterization) test [16].
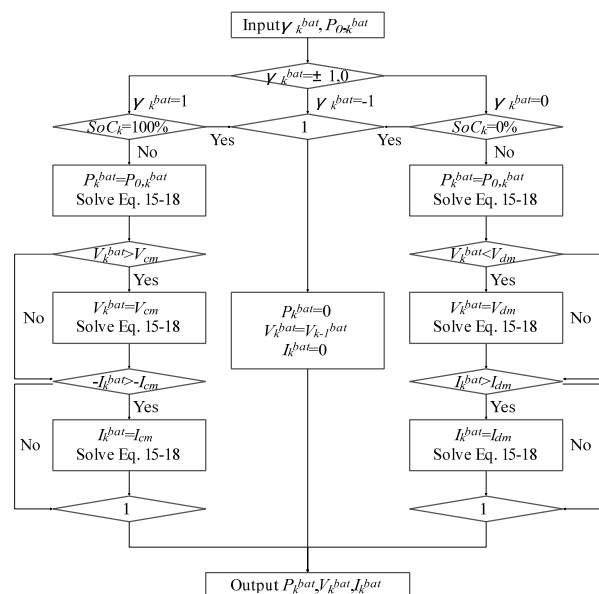

Figure 5. Flow chart of the battery model output calculation

$$V_k^{bat} = V_{oc,k} - V_{b,k} - V_{p,k} - I_k^{bat} R_{o,k} \quad (15)$$

$$C_{b,k} \frac{V_{b,k} - V_{b,k-1}}{\Delta t} = I_k^{bat} \quad (16)$$

$$C_{p,k} \frac{V_{p,k} - V_{p,k-1}}{\Delta t} = I_k^{bat} - \frac{V_{p,k}}{R_{p,k}} \quad (17)$$

$$P_k^{bat} = I_k^{bat} V_k^{bat} \quad (18)$$

Equation 19 applies an Amper-Hour integral method to calculate the current SoC, where C_m is the maximal capacity of the battery [13, 15].

$$SoC_k = SoC_{k-1} - \frac{I_{k-1}^{bat} \Delta t}{C_m} \quad (19)$$

Figure 5 shows the calculation process of output power P^{bat}. γ^{bat} is the indicator of the charge/discharge state (1-charge, 0-discharge, -1-no change) and P_0^{bat} is the system power demand from the battery. V_{cm}, V_{dm}, I_{cm} and I_{dm} are the charge/discharge control limits of the voltage and current.

4.2 Super-Capacitor Model

The RC network always simulates a double-layer capacitor. This paper applies a circuit as shown in Figure 6 [17]. The first branch, consisting of R_i and C_i, interprets the transient stage of five seconds after an abrupt change. The second branch, consisting of R_d and C_d, interprets the retardant stage of the follow-up 20 minutes after the abrupt change. R_l reflects the leakage in a static stage.

Like the battery, the super-capacitor model includes discrete equations [17, 18]. The transient stage is described with Equation 20, while Equation 21 illustrates the transient stage. All the model parameters, R_i, C_{i0}, C_{i1}, R_d, C_d and R_l can be determined from the constant current charge test [19].
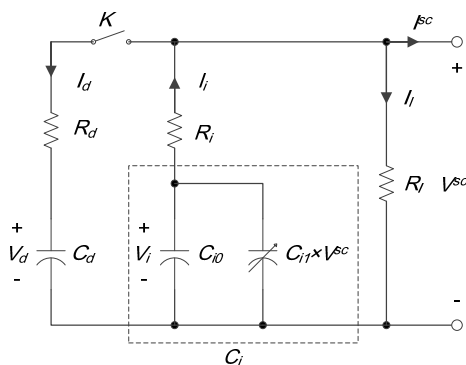

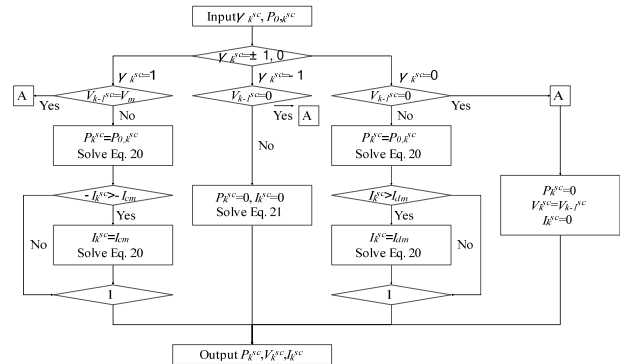**Figure 6.** Super-capacitor model – Parallel RC Network

Figure 7. Flow chart of the super-capacitor model output calculation

$$\begin{cases} I_k^{sc} = I_{i,k} - I_{l,k} \\ V_k^{sc} = I_{l,k} R_l \\ V_k^{sc} = V_{i,k} - I_{i,k} R_i \\ -I_{i,k} = \left(C_{i0} + C_{i1} V_k^{sc} \right) \dfrac{V_{i,k} - V_{i,k-1}}{\Delta t} \\ P_k^{sc} = I_k^{sc} V_k^{sc} \end{cases} \quad (20)$$

$$\begin{cases} I_{i,k} = I_{d,k} + I_{l,k} \\ V_k^{sc} = I_{l,k} R_l \\ V_k^{sc} = V_{i,k} - I_{i,k} R_i \\ -I_{i,k} = \left(C_{i0} + C_{i1} V_k^{sc} \right) \dfrac{V_{i,k} - V_{i,k-1}}{\Delta t} \\ V_k^{sc} = V_{d,k} + I_{d,k} R_d \\ I_{d,k} = C_d \dfrac{V_{d,k} - V_{d,k-1}}{\Delta t} \end{cases} \quad (21)$$

Similarly to the Li-ion battery, a calculation process for super-capacitor output power is shown in Figure 7.

5. Energy Output Module

Energy output modules can be any kinds of load. A typical one is the wireless sensor network, which operates intermittently and periodically [1]. Noting the period as T and duty cycle of active status as D, the output power demand can be expressed as Equation 22.

$$P_0^{ch}(t) = \begin{cases} P_{active}, & 0 < t < DT \\ P_{sleep}, & DT < t < T \end{cases} \quad (22)$$

6. Energy Management Module

The energy management module is the core part of providing a strategy of power distribution. The structure is shown in Figure 8.

The energy lost term P^{pm} is illustrated in Equation 23, with η^* being the efficiency of the relevant DC/DC device.

$$P^{pm} = \left(1 - \eta^{pv}\right) P^{pv} + \left(1 - \eta^{pz}\right) P^{pz} + \left(\frac{1}{\eta^{ch}} - 1\right) P^{ch} + P_{other} \quad (23)$$
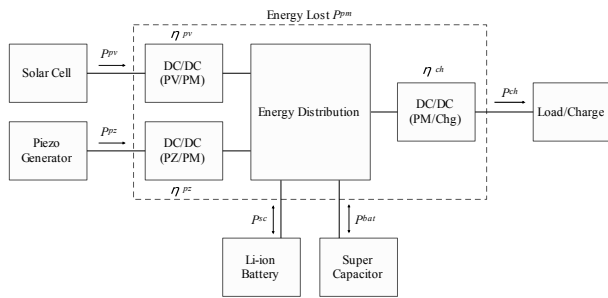
Figure 8. Energy management module

Hybrid energy systems with multiple input sources and storage units require a power distribution strategy to manage the energy flux. A General Coefficient Distribution Method (GCDM) is proposed to simulate the strategy. GCDM can be interpreted with Equation 24 and 25, where a certain combination of β^* and α_i^* presents a relative distribution strategy.

$$P_0^{bat} = \beta^{bat} \frac{1}{\eta^{ch}} P^{ch} - \alpha_1^{bat} \eta^{pv} P^{pv} - \alpha_2^{bat} \eta^{pz} P^{pz} \qquad (24)$$

$$P_0^{sc} = \beta^{sc} \frac{1}{\eta^{ch}} P^{ch} - \alpha_1^{sc} \eta^{pv} P^{pv} - \alpha_2^{sc} \eta^{pz} P^{pz} \qquad (25)$$

The sum of P_0^{bat} and P_0^{sc} should match the gap of system power demand P_0 :

$$P_0 = \frac{1}{\eta^{ch}} P^{ch} - \eta^{pv} P^{pv} - \eta^{pz} P^{pz} \qquad (26)$$

In other words, the distribution strategy is supposed to accord with the principle of power conservation. As a result, the coefficients in GCDM should be restricted with Equation 27:

$$\sum_s \beta^s = \sum_s \alpha_i^s = 1 \qquad (27)$$

Two common management strategies are raised here to explain the implementation of GCDM, with definitions of trigger conditions and values of β^* and α_i^*, as shown in Table 1. Other strategies can be modelled with different definitions of trigger conditions, β^s and α_i^s .

Strategy	Triggle Conditions	β^{bat}	α_1^{bat}	α_2^{bat}	β^{sc}	α_1^{sc}	α_2^{sc}
Parallel Storage	$\begin{cases} P_0 > 0 \\ V^{sc} > V^{bat} \end{cases}$ or $\begin{cases} P_0 < 0 \\ V^{sc} < V^{bat} \end{cases}$	0	0	0	1	1	1
	$\begin{cases} P_0 > 0 \\ V^{sc} < V^{bat} \end{cases}$ or $\begin{cases} P_0 < 0 \\ V^{sc} > V^{bat} \end{cases}$	1	1	1	0	0	0
Super Capacitor First	$\begin{cases} P_0^{sc} > 0 \\ V^{sc} > 0 \end{cases}$ or $\begin{cases} P_0^{sc} < 0 \\ V^{sc} < V_{max} \end{cases}$	0	0	0	1	1	1
	$\begin{cases} P_0^{sc} > 0 \\ V^{sc} = 0 \end{cases}$ or $\begin{cases} P_0^{sc} < 0 \\ V^{sc} = V_{max} \end{cases}$	1	1	1	0	0	0

Table 1. Two power management strategies modelled using the General Coefficient Distribution Method

The simplest design is to have a battery and super capacitor parallel in the circuit. If the system asks for extra power from storage ($P_0 > 0$), the unit with a higher voltage will at first discharge and its coefficients will be one while others' are 0; on the contrary in case of a charge ($P_0 < 0$).

Another strategy example is to have super capacitor prior to charge or discharge, since a capacitor presents a better performance in instantaneous high-power charging /discharging. In case of a positive power gap ($P_0 > 0$), the distribution coefficient can be firstly defined as $\beta^{sc} = \alpha_1^{sc} = \alpha_2^{sc} = 1$, $\beta^{bat} = \alpha_1^{bat} = \alpha_2^{bat} = 0$ when $V^{sc} > 0$, and won't change to $\beta^{sc} = \alpha_1^{sc} = \alpha_2^{sc} = 0$, $\beta^{bat} = \alpha_1^{bat} = \alpha_2^{bat} = 1$ until $V^{sc} = 0$ (super capacitor fully discharged).

7. Summary

An accurate and comprehensive electrical model has been proposed to simulate the power flux of a hybrid energy system (HES). Photovoltaic and piezo-generators are the primary choice of harvesters in this model. As hybrid energy storage, a Li-ion battery and super-capacitor are included and a status identification and output calculation process is respectively illustrated. A generalized energy management strategy, the General Coefficient Distribution Method, is approached with combinations of distribution factors. This system model can be reproduced into other HES by alternating the relevant harvester and storage modules and be simulated under a Matlab environment. With the help of an HES model, hardware development can be significantly accelerated and more oriented with adjusted parameters.

8. References

[1] Penella M.T, Gasulla M (2007). A Review of Commercial Energy Harvesters for Autonomous Sensors. IEEE Instrumentation and Measurement Technology Conference.

[2] Chen C, Tang Y-C, Wang H-Y, Wang Y-D (2013). A Review of Fabrication Options and Power Electronics for Flapping-Wing Robotic Insects. International Journal of Advanced Robotic Systems, 10(151).

[3] Beeby S, White N (2010). Energy Harvesting for Autonomous Systems. Norwood: Artech House. pp. 91-134.

[4] Yu H-Y, Li Y-Q, Shang Y-H, Su B (2009). Experimental Investigation and Optimization on Photovoltaic-Thermoelectric Hybrid Power Source. Acta Energiae Solaris Sinica, 30(4): 436-440.

[5] King D.L, Boyson W.E, Kratochvil J.A (2003). Photovoltaic Array Performance Model. Report of Sandia National Laboratories.

[6] De Soto W, Klein S.A, Beckman W.A (2005). Improvement and Validation of a Model for

Photovoltaic Array Performance. Solar Energy, 80(1): 78-88.

[7] Dzimano G (2008). Modeling of Photovoltaic Systems. MS Thesis, Ohio State University.

[8] Mitcheson P.D, Green T.C, Yeatman E.M, Holmes A.S (2004). Architectures for Vibration-Driven Micropower Generators. Journal of Micro-Electro-Mechanical Systems, 13(3): 429-440.

[9] Roundy S.J (2003). Energy Scavenging for Wireless Sensor Nodes with a Focus on Vibration to Electricity Conversion. Ph.D Thesis, University of California, Berkeley.

[10] Erturk A, Inman D.J (2008). On Mechanical Modeling of Cantilevered Piezoelectric Vibration Energy Harvesters. Journal of Intelligent Material Systems and Structures, 19(11): 1311-1325.

[11] Dong Y (2008). Vibration Piezoelectric Micro Generator and Application in the Machinery Fault Monitoring System. MS Thesis, Chongqing University, China.

[12] Tabesh A, Fréchette L.G (2010). A Low-Power Stand-Alone Adaptive Circuit for Harvesting Energy from a Piezoelectric Micropower Generator. IEEE Transactions on Industrial Electronics, 57(3): 840-849.

[13] Johnson V.H (2002). Battery Performance Models in ADVISOR. Journal of Power Sources, 110(2): 321-329.

[14] Chen M, Rincón-Mora G.A (2006). Accurate Electrical Battery Model Capable of Predicting Runtime and I-V Performance. IEEE Transactions on Energy Conversion, 21(2): 504-511.

[15] Lu J-X, Lin C-T, Chen Q-S, Han X-D (2006). Comparison Study of 3 Types of Battery Models for Electrical Vehicle. Power Source Technology, 30(7): 535-538.

[16] Hunt G (2001). PNGV Battery Test Manual. Report of Idaho National Engineering & Environmental Laboratory.

[17] Zubieta L, Bonert R (2000). Characterization of Double-Layer Capacitors for Power Electronics Applications. IEEE Transactions on Industry Applications, 36(1): 199-205.

[18] Yang H-Z, Zhang Y (2011). Evaluation of Supercapacitor Models for Wireless Sensor Network Applications. 5th International Conference on Signal Processing and Communication Systems.

[19] Xiong R, He H-W, Zhang X-W (2010). Modeling of Ultracapacitor based on Experimental Data. Vehicle and Power Technology, 4: 25-28.